Energy Conversion and Management 150 (2017) 515–531

Contents lists available at ScienceDirect

Energy Conversion and Management

journal homepage: www.elsevier.com/locate/enconman

Characterization of PVT systems equipped with nanofluids-based collector from entropy generation

Seyed Reza Maadi[a,1], Arman Kolahan[a,1], Mohammad Passandideh-Fard[a,*], Mohammad Sardarabadi[a], Reza Moloudi[b]

[a] Department of Mechanical Engineering, Ferdowsi University of Mashhad, Mashhad, Iran
[b] Division of Thermal and Fluids Engineering, Nanyang Technological University, Singapore, Singapore

ARTICLE INFO

Keywords:
Photovoltaic thermal system
Nanofluid
Thermal and frictional entropy generation
Exergy efficiency
Heat transfer
Thermo-physical properties

ABSTRACT

In this study, a PVT system equipped with a nanofluid-based collector is investigated from entropy generation viewpoint. The purpose of this study is characterizing a PVT system in order to enhance its performance. For this purpose, the effects of adding nanoparticles on entropy generation are investigated using a 2D-transient numerical model validated with experimental measurements. The experiments were performed for various nanofluids (Al_2O_3/water, TiO_2 /water and ZnO /water by 0.2 wt%, and SiO_2 /water by 1 wt% and 3 wt%) on a PV system equipped with a serpentine collector tube to increase its efficiency. A good agreement is observed between model calculations and those of the measurements. The effect of various metallic and metalloid nanofluid mass fractions on thermal (locally) and frictional fluid entropy generations, and the total entropy generation of the PVT system are investigated. The effects of various nanofluids on thermo-physical properties, coolant fluid heat transfer, and energy and exergy efficiencies are also examined. The results show that adding nanoparticles improves the thermal exergy efficiency of the system. ZnO /water had the highest and SiO_2 /water had the lowest thermal exergy efficiency. In addition, it is observed that by increasing the mass fraction of metallic-water nanofluids (Al_2O_3, TiO_2 and ZnO /water) in the range considered in this study, less entropy is generated due to the improvement made in the nanofluid thermo-physical properties. For Al_2O_3 /water nanofluid, the best performance in terms of thermal and total entropy generation is obtained. The ZnO /water nanofluid is also found to generate the least frictional entropy generation. However for metalloid nanofluid considered in this study (SiO_2/water nanofluid) is found to have the most entropy generation which is not favorable.

1. Introduction

Nowadays, using renewable sources of energy such as solar energy in many applications is becoming more and more popular. Sun is one of the infinite sources of energy; almost 51% of the incoming solar energy towards the earth reaches the earth surface and the rest is absorbed and reflected by the atmosphere [1]. Solar energy is not concentrated at a certain place and time; for this reason, it is necessary to find a way to collect it efficiently. Solar energy does not have the disadvantages of fossil fuels such as pollution and global warming [2]. Three common types of solar energy systems include solar collectors, photovoltaic cells and photovoltaic/thermal (PVT) units widely used to generate electricity and produce thermal energy. A photovoltaic thermal unit may be regarded as a hybrid system that converts radiant energy into electricity and heat, simultaneously. It has been determined that increasing the PV cells temperature by 1 degree at the crystalline silicon cells, the amorphous silicon cells, and the c-Si cells will reduce the electrical efficiency by 0.5%, 0.25% and 0.45%, respectively [3–5]. In addition, if the thermal stress on the PV cells remains for a long period of time, it can damage the module [6]. The technical performance of a PVT system is usually evaluated by energy and exergy efficiencies [7]. The dual functions of the PVT system results in a higher performance compared to that of a PV unit.

Several methods simulated PVT system have been introduced to control the PV cell temperature in order to increase the electrical efficiency and employ the absorbed heat. Bhattarai et al. [8] simulated one-dimensional transient model by commercial software (MATLAB) for water-cooled PVT system. They investigated the total efficiency of the PVT is almost 16% higher than the solar collector system. Rejeb et al. [9] investigated PVT system numerically by FORTRAN. They found in a water-cooled PVT system by increasing the solar radiation can achieve high thermal efficiency and high conduction coefficient

* Corresponding author.
E-mail address: mpfard@um.ac.ir (M. Passandideh-Fard).
[1] These authors have equal contribution in the paper.

http://dx.doi.org/10.1016/j.enconman.2017.08.039
Received 12 May 2017; Received in revised form 13 August 2017; Accepted 14 August 2017

Nomenclature

Symbols

d	diameter m
δ	thickness m
ρ	density kg/m^3
C	specific heat capacity $J/kg\ K$
k	thermal conductivity $W/m\ K$
r	packing factor –
α	absorptivity –
ε	emissivity –
τ	transmittance –
W	width m
L	length m
T	temperature K
μ	viscosity $Pa.\ s$
φ	nanofluid volume fraction –
ΔP	pressure drop Pa
G	solar radiation W/m^2
h	heat transfer coefficient W/m^2K
h_f	frictional head loss m
δx	cell width m
δy	cell length m
t	Time s
η	efficiency –
η_{II}	exergy efficiency –
V	velocity m/s
Nu	Nusselt Number –
Re	Reynolds Number –
Pr	Prandtl Number –
E	energy W/m^2
Ex	exergy W/m^2
S	entropy J/K
P	perimeter m
M	mass kg
$wt\%$	nanofluid mass fraction –

Abbreviations

PV	photovoltaic
PVT	photovoltaic/thermal

Subscripts

nf	nanofluid
f	fluid
p	nanoparticle
g	glass
rad	radiation
env	environment
sky	sky
$wind$	wind
amb	ambient
$cond$	conduction
pv	photovoltaic
el	electrical
ab	absorber
in	insulation
t	tube wall
$conv$	convection
th	thermal
o	outlet
i	inlet
gen	generation
$inst$	installation
inv	inverter
sub	subsidy

between the photovoltaic module and the absorber plate. They also found by increasing inlet water temperature the thermal efficiency and electrical efficiency will decrease. Yazdanpanahi et al. [10] investigated the water-cooled PVT system experimentally and numerically (one dimensional steady) from the 2nd law of thermodynamic. At their study they found at a constant solar intensity 700 $\frac{W}{m^2}$, by increasing mass flow rate from 0.001 to 0.002 kg/s exergy efficiency will increase from 10% to 13.95% while by increasing mass flow rate bigger than 0.002 kg/s exergy efficiency will drop down. Also, they found at a 0.002 kg/s mass flow rate by increasing solar radiation intensity from 0 to 1000 $\frac{W}{m^2}$ their exergy efficiency increase exponentially from 0 to 15.5%. Singh et al. [11] used a genetic algorithm–fuzzy system (GA-FS) for optimization of a glazed photovoltaic thermal (PVT) system and improvement of the overall exergy efficiency. They obtained an overall exergy efficiency of 15.82% with the GA–FS approach which was 1.27% and 5.40% more than the efficiency of the system optimized with the GA and un-optimized system, respectively. In another study [12], they optimized a dual channel semitransparent PVT module by using the fuzzyfied genetic algorithm (FGA). They reported an improvement of 1.13% in electrical efficiency and 12.21% improvement in overall exergy efficiency compared to those of un-optimized system. Yazadanifard et al. [13] numerically simulated a water-cooled PVT system by a commercial software (MATLAB) in both laminar and turbulent flow regimes. They found that while the total energy efficiency was higher in turbulent regime, the laminar regime was more efficient from the exergy viewpoint.

Using nanoparticles in a fluid is an efficient method to enhance its heat transfer performance because nanoparticles can improve the thermo-physical base-fluid properties. Sardarabadi et al. [2] experimentally investigated the effects of SiO_2/water (Silicon Dioxide) nanofluid as a cooling system. They found that using a nanofluid by 1 wt% and 3 wt% increased the overall efficiency by 3.6% and 7.9%, respectively, compared to that of pure water. They also observed by adding a thermal collector to a PV system that the total exergy of the PVT with pure water, 1 wt% and 3 wt% SiO_2/water nanofluid was increased by 19.36%, 22.61% and 24.31%, respectively. Rejeb et al. [14] numerically investigated the effects of nanofluids on electrical and thermal performance of an uncovered PVT system. They used Al_2O_3 (Aluminum Oxide), Cu nanoparticles in water and ethylene glycol. They found that nanoparticles improve the thermo-physical properties of base-fluid and increase the heat transfer between the tube and the fluid. They concluded that the Cu/water nanofluid had a better performance between other tested nanofluids. Sardarabadi et al. [15] investigated the effects of various metal-oxidewater nanofluids as coolant in their experiments. They examined Al_2O_3, TiO_2 (Titanium Dioxide) and ZnO /water (Zinc Oxide) by 0.2 wt%. They showed that the PVT thermal performance is highly and electrical efficiency is slightly dependent on the mass fraction of the nanoparticles. Khanjari et al. [16] used the FLUENT software to investigate the effect of nanofluid on the PVT performance. They showed that increasing nanofluid volume fraction increases the heat transfer coefficient and efficiency. They showed that depending on the inlet fluid velocity, for Al_2O_3 /water nanofluid at $\varphi = 5\%$ (volume fraction), the heat transfer coefficient increases 8–10% compared to that of the pure water. For Ag/water nanofluid with the same concentration, the increase of the heat transfer coefficient was more pronounced (28–45%). More CFD works and dynamic model simulations

for the flat plate PVT systems can be seen in the review article of Tagliafico et al. [17]. As can be seen from the above literature review on a PVT system equipped with nanofluid base collector, the effect of thermo-physical properties of different nanofluids on the exergy efficiency and heat transfer were rarely investigated.

Based on the 2nd law of thermodynamic, entropy generation analysis can be useful for reducing the lost work and optimizing the system optimization [18]. Moghadami et al. [19] used CFD simulations to investigate the change of entropy generation by adding Al_2O_3 nanoparticles to the fluid in a circular tube with a constant heat flux. They investigated different nanoparticles concentration vs. Reynolds number. Their results showed that in a laminar regime, by using nanofluids, the reduction of entropy due to the heat transfer was significantly more than the increase of entropy due to friction. Therefore, they concluded that using Al_2O_3 /water nanofluid instead of pure water at low Reynolds number can decrease the total system entropy. Alim et al. [20] investigated analytically the entropy generation of a solar nanofluid based collector. They used Al_2O_3, CuO, SiO_2, and TiO_2 nanoparticles in water as a base-fluid. They reported a conclusion similar to that of Moghadami et al. [19] for the effect of adding nanoparticles on entropy generation on the system. They found CuO /water nanofluid to have the best performance among various nanofluids they considered. More details of entropy generation in collectors can be seen in the review paper of Mahian et al. [21].

In this paper, a combined experimental and numerical research is performed to study the entropy generations and efficiencies of a PVT nanofluid-based collector system. From the comprehensive literature review mentioned above, the focus of most researchers in this field has been the entropy generation analysis in solar thermal collectors rather than PVT systems. Few studies are available in the literature on the effect of thermo-physical properties of nanofluids on the entropy generation and pressure drop analyses in PVT nanofluid-based collectors for various mass fractions. In this research, therefore, a comparison is performed between metalloid and metal oxides nanoparticles with different mass fractions in a nanofluid from the thermodynamics viewpoint based on the 2nd law (i.e., thermal, frictional and total entropy generations; and thermal and electrical exergies). The main focus of this study is to investigate the effect of nanofluids thermo-physical properties on the entropy generations (local and total of thermal entropy generation and total of frictional entropy generation) by adding different nanoparticles. These analyses are accomplished based on the thermal properties of each nanofluid for various mass fractions.

The experimental setup used in this study consists of a PVT water-cooled system (as a reference system) and a PVT nanofluid based collector system. For the numerical part, a 2D transient model is developed (in Fortran programming) to simulate a PVT nanofluid-based collector. No commercial software was used in this study. The selected nanofluids include SiO_2/water, TiO_2/water, ZnO/water, and Al_2O_3/water.

2. Experimental setup

A view and schematic diagram of the experimental setups are shown in Figs. 1 and 2. The setup in the experiment consists of a 40 W monocrystalline silicon photovoltaic module (Suntech Co., China). In the system, referred as PVT, the photovoltaic module is equipped with a copper sheet and tube collector.

In the PVT, a shell and tube heat exchanger is used to cool the working fluids in a closed flow circuit after having absorbed the heat in the collectors. A working fluid with a mass flow rate of 30 kg/h is used in the PVT system. The details of the selection procedure for the fluids mass flow rate can be seen elsewhere [2]. The working fluids considered in the experiments are Al_2O_3/water, TiO_2/water and ZnO/water by 0.2 wt%, and SiO_2/water by 1 wt% and 3 wt%. Nanofluids are stabilized with an ultrasound mechanism and acetic acid (CH3COOH) as a surfactant. The daily measured data is collected from 9:30 am to 3:30 pm on selected days at the Ferdowsi University of Mashhad, Mashhad, Iran (Latitude: 36o and Longitude: 59o). In the experiments, the tilt angle of the collector is set at a constant value of 30 degrees (the slope with respect to the horizontal surface while the collector is facing south).

It should be noted that no sedimentation of nanoparticles in the suspension was observed after 7 days. Fluid flow temperatures at the inlet and outlet of the heat exchanger and that of the collector are measured by K-type and RTD sensors. The collected data of the K-types are then stored by a data logger (Testo, 177 T4). The surface temperature of different points (middle and four corners) of the PV unit are measured by a portable K-type surface thermocouple where the maximum value is reported as the PV surface temperature. Digital multimeters are used to measure the short-circuit and load currents, and the open-circuit and load voltages. The total incident radiation is measured by a solar power meter (TES-1333) positioned parallel to the photovoltaic surfaces. The working fluid mass flow rates are controlled and measured by a rotary flow meter. In order to determine the reliability of the experiments, an uncertainly analysis is performed for the measured parameters and electrical efficiency [2]. If R is a function of 'n' independent linear parameters as $R = R(\nu_1,\nu_2,...,\nu_n)$, the uncertainty of function R is defined as:

$$\delta R = \sqrt{\left(\frac{\partial R}{\partial \nu_1}\delta\nu_1\right)^2 + \left(\frac{\partial R}{\partial \nu_2}\delta\nu_2\right)^2 + ... + \left(\frac{\partial R}{\partial \nu_n}\delta\nu_n\right)^2} \quad (1)$$

where δR is the uncertainty of function R, $\delta\nu_i$ the uncertainty of parameter ν_i, and $\frac{\partial R}{\partial \nu_i}$ is the partial derivative of R with respect to parameter ν_i. The uncertainty of the experiments was found to be less than 5% for all cases in this paper. More details of the measuring instruments and experimental uncertainties can be found elsewhere [2].

3. Mathematical model

In this paper, the effect of adding different nanoparticles on the performance of the PVT system is investigated both numerically and experimentally. The results of numerical solutions are compared with those of the measurements. The numerical model developed in this study is unsteady and two-dimensional. The schematic diagram of the model is shown in Fig. 2b.

3.1. Assumptions

The main purpose of modeling is to find the temperature distribution of the PV unit and the collector in order to analyze the system from both 1st and 2nd laws of thermodynamics. The type of working fluid plays an important role in the system efficiency and entropy generation. The main assumptions used in the mathematical model are as follows:

- Fluid flow in the collector is incompressible, laminar, one

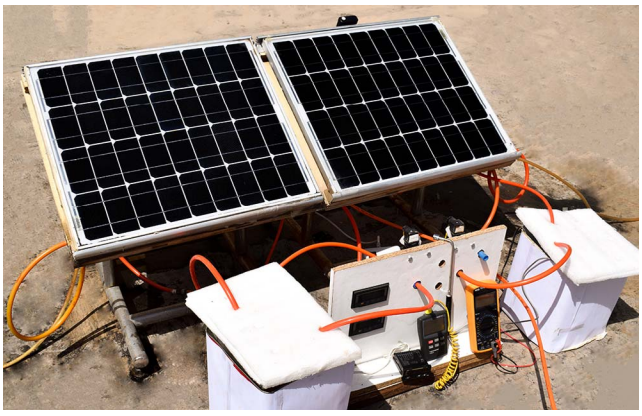

Fig. 1. The experimental setup.

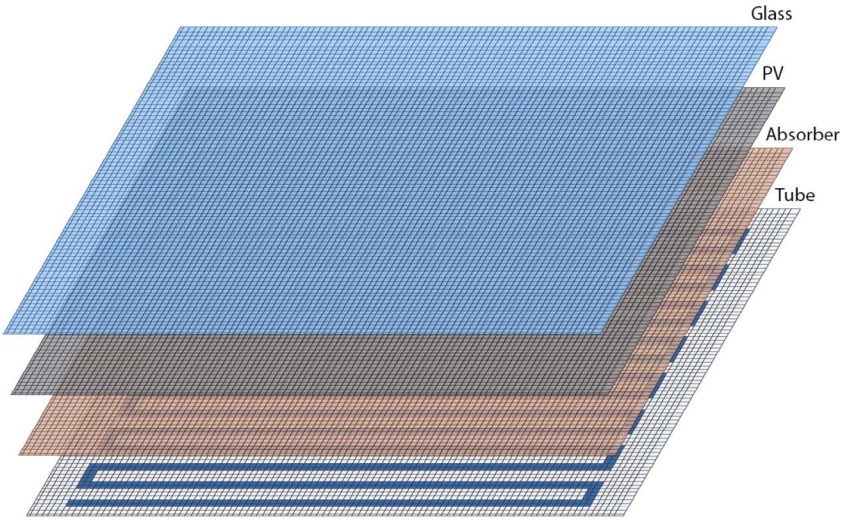

(a) the PVT system plates and its meshes

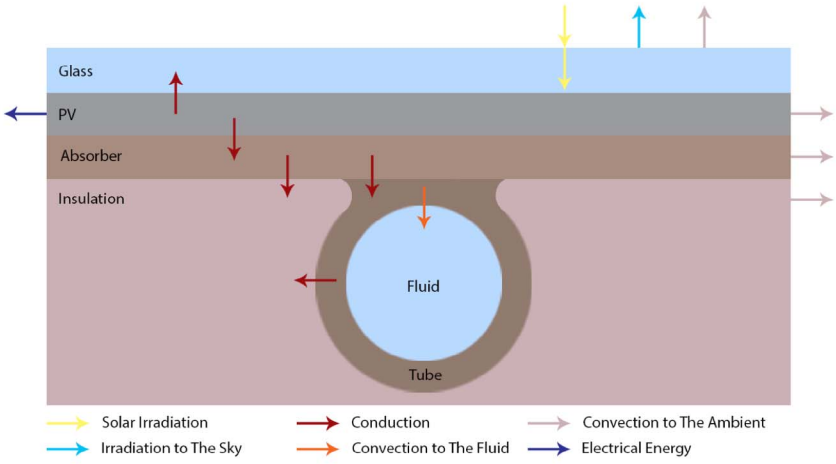

(b) The schematic diagram of the PVT model and its layers and heat transfers

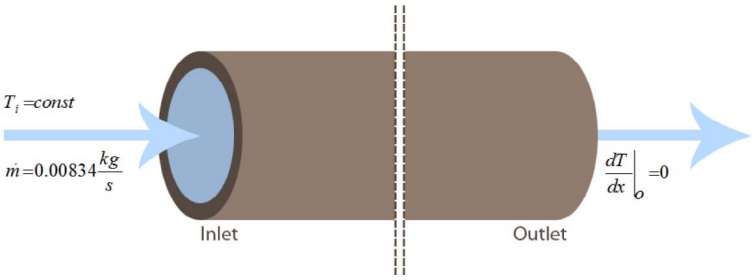

(c) The boundary condition of the tube

Fig. 2. (a) the PVT system plates and its meshes. (b) The schematic diagram of the PVT model and its layers and heat transfers. (c) The boundary condition of the tube.

dimensional (axial) and uniform.

- The sky is assumed a black body with a temperature of T_{sky}.
- The various layers are assumed thin with no temperature gradient within their thickness.
- Solar radiation is perpendicular to the photovoltaic plate.
- Nanofluid assumed as a single phase fluid (both the fluid phase and particles are in a thermal equilibrium state and they flow at the same velocity).

3.2. Geometry and properties

According to the Fig. 2a, the collector type is serpentine. The properties and geometry of the model developed in this study is listed in Table 1.

Pure water is selected as the base-fluid with temperature dependent properties given in the relations provided in Table 2.

By varying the water temperature from 30 to 60 °C, the net changes of density, viscosity, thermal conductivity, and specific heat capacity are in the range of 1, 42, 6 and 0.1% respectively. The nanofluid is modeled as a single phase with thermo-physical properties obtained based on the equations given in this section [22].

$$\rho_{nf} = \varphi\rho_p + (1-\varphi)\rho_f \tag{2}$$

where ρ_{nf} is nanofluid density, ρ_f and ρ_p are base-fluid and nanoparticle

Table 1
The PVT system geometry and properties.

Glass	Tube	Absorber plate
$\delta_g = 3$ mm	$d_t = 8$ mm	$\delta_{ab} = 0.3$ mm
$\rho_g = 2200 \frac{kg}{m^3}$	$\delta_t = 1$ mm	$\rho_{ab} = 8920 \frac{kg}{m^3}$
$C_g = 480 \frac{J}{kgK}$	$\rho_t = 8920 \frac{kg}{m^3}$	$C_{ab} = 385 \frac{J}{kg\ K}$
$k_g = 1.1 \frac{W}{mK}$	$C_t = 385 \frac{J}{kg\ K}$	$k_{ab} = 398 \frac{W}{mK}$
$\alpha_g = 0.05$	$k_t = 398 \frac{W}{mK}$	$R''_{ab \to pv} = 5 \times 10^{-7} \frac{K}{W}$
$\varepsilon_g = 0.92$	$\dot{m} = 0.00834 \frac{kg}{s}$	
$\tau_g = 0.936$		

Dimensions	Photovoltaic	
$W = 0.54$ m	$\delta_{pv} = 0.3\ mm$	$r_{pv} = 0.94$
$L = 0.63$ m	$\rho_{pv} = 2330 \frac{kg}{m^3}$	$\alpha_{pv} = 0.95$
	$C_{pv} = 700 \frac{J}{kg\ K}$	$\beta_{pv} = 0.0045\ K^{-1}$
	$k_{pv} = 84 \frac{W}{mK}$	$\eta_{el,0} = 16\% at 298$ K
		$R''_{g \to pv} = 3.8 \times 10^{-4} \frac{K}{W}$

Table 2
The base fluid (water) properties versus temperature.

Density $\frac{kg}{m^3}$	$\rho_f = 1000 - 0.0178\lvert T - 277\rvert^{1.7} \pm 0.2\%$ [30]
Viscosity $\frac{kg}{m.s}$	$\mu_f = 1.788 \times 10^{-3} \exp(-1.704 - \frac{1448.538}{T} + \frac{521926.58}{T^2})$ [30]
Thermal Conductivity $\frac{W}{mK}$	$k_f = -8.01 \times 10^{-6}(T-273)^2 + 1.94 \times 10^{-3}(T-273) + 0.563$ [16]
Specific Heat Capacity $\frac{J}{kgK}$	$C_f = 4.1855 \times 10^3 \left(0.966185 + 0.0002874\left(\left(\frac{T-173}{100}\right)^{5.26}\right)\right) + 0.011160 \times 10^{-0.036(T-273)}$ [16]

densities and φ is nanofluid volume fraction that can be calculated as:

$$\varphi = \frac{\frac{m_p}{\rho_p}}{\frac{m_p}{\rho_p} + \frac{m_f}{\rho_f}} \tag{3}$$

where m_p and m_f are the mass of nanoparticle and fluid, respectively.

The heat capacity of nanofluid is determined by:

$$C_{nf} = \frac{\varphi \rho_p C_p + (1-\varphi)\rho_f C_f}{\rho_{nf}} \tag{4}$$

where C_{nf}, C_f and C_p is nanofluid, base-fluid and nanoparticle specific heat capacities, respectively.

The viscosity of nanofluid is given by Brinkman [23] as:

$$\mu_{nf} = \frac{\mu_f}{(1-\varphi)^{2.5}} \tag{5}$$

where μ_{nf} and μ_f are nanofluid and base-fluid viscosity, respectively.

To calculate thermal conductivity, the Maxwell relations [24] is used:

$$k_{nf} = \frac{k_p + 2k_f + 2\varphi(k_p - k_f)}{k_p + 2k_f - \varphi(k_p - k_f)} k_f \tag{6}$$

where k_{nf}, k_f and k_p are thermal conductivities of nanofluid, base-fluid and nanoparticle respectively.

The properties of nanoparticles used for the modeling are summarized in Table 3.

3.3. Governing equations

To find temperatures at all points in the entire PVT system under consideration, the energy equations for all plates (Fig. 2) need to be solved simultaneously. There are three plates of glass, PV and absorber under which the tube that carries the cooling fluid is attached. The tube is covered with insulation (see Fig. 2b). The energy equations written in this section are only provide for an inner computational cell. Special considerations are required at the boundaries.

For the glass plate, the irradiation from the sun and the radiation of the plate to the sky must be considered. The convection heat transfer to the surrounding ambient and the conduction to the PV plate should also be included in the energy equation, given as:

$$\rho_g \delta_g c_g \frac{dT_g}{dt} = \alpha_g G - h_{rad,g \to env}(T_g - T_{sky}) - h_{wind}(T_g - T_{amb}) + U_{cond,g \to pv}(T_{pv} - T_g) + \delta_g \nabla . (k_g \nabla T_g) \tag{7}$$

where ρ, α, δ and c are density, absorptivity, thickness and specific heat coefficient. G is solar radiation per unit area and subscript g refers to the glass. $h_{rad,g \to env}$, h_{wind} and $U_{cond,g \to pv}$ are heat transfer coefficient of radiation to the environment, convection heat transfer coefficient to the ambient, and total heat transfer coefficient between glass and PV plates, respectively. T_{sky}, T_{amb}, T_{pv} and T_g are the temperatures corresponding to the sky, ambient, PV plate and the cover glass, respectively.

The above equation is solved numerically using an implicit formulation where the diffusion term ($\delta_g \nabla \cdot (k_g \nabla T_g)$) is spatially discretized by a center-differencing scheme. The discretized equations are solved using the TDMA numerical method.

For the sky temperature, the following equation [25] such as:

$$T_{sky} = 0.0552 T_{amb}^{1.5} \tag{8}$$

The equivalent heat transfer coefficient of radiation to the environment is given by [14]:

$$h_{rad,g \to env} = \varepsilon_g \sigma (T_g^2 + T_{sky}^2)(T_g + T_{sky}) \tag{9}$$

where ε_g and σ are emissivity of glass and Stefan Boltzman constant, respectively.

The convection heat transfer coefficient to the ambient is calculated based on the following equation that considers the wind speed [26]:

$$h_{wind} = \begin{cases} 5.7 + 3.8 V_{wind}, V_{wind} < 5 \frac{m}{s} \\ 6.47 + V_{wind}^{0.78}, V_{wind} \geqslant 5 \frac{m}{s} \end{cases} \tag{10}$$

where V_{wind} is the local wind speed. In this research, the wind is assumed to have an average speed of $1 \frac{m}{s}$.

The total heat transfer coefficient between glass and PV plate is calculated as:

$$U_{cond,g \to pv} = \frac{1}{\frac{\delta_g}{2k_g} + \frac{\delta_{pv}}{2k_{pv}} + R''_{g \to pv}} \tag{11}$$

where $R''_{g \to pv}$ is the thermal contact resistance per unit area between the glass and PV plate.

For the PV plate, it receives the solar radiation transmitted from the glass plate and converts part of the energy to electricity and the rest are transferred to both the glass and absorber plates. Therefore, the energy equation is written as:

Table 3
The nanoparticles properties.

Nanoparticle	Density $\frac{kg}{m^3}$	Specific heat capacity $\frac{J}{kgK}$	Thermal conductivity $\frac{W}{mK}$
Al_2O_3	3970	765	40
TiO_2	4250	686	8.9
ZnO	5600	495	13
SiO_2	2170	680	1.3

$$\rho_{pv}\delta_{pv}C_{pv}\frac{dT_{pv}}{dt} = \alpha_{pv}\tau_g G - U_{cond,pv\to ab}(T_{pv}-T_{ab}) - U_{cond,g\to pv}(T_{pv}-T_g) - \dot{E}_{el} + \delta_{pv}\nabla.(k_{pv}\nabla T_{pv}) \quad (12)$$

where τ_g is the transmittance of glass and subscript pv refers to the PV plate; $U_{cond,pv\to ab}$ is the total heat transfer coefficient between the PV and absorber plate calculated similarly as of Eq. (11). $\dot{E}_{el}$ is the rate of generated electricity per unit area which depends on the PV plate temperature based on the following relation [4]:

$$\dot{E}_{el} = -K_1\beta T_{pv} + K_2$$
$$K_1 = \tau_g G\eta_0 r$$
$$K_2 = K_1(1 + 298\beta) \quad (13)$$

where β, K_1 and K_2 are constant coefficients and η_0 is the electrical efficiency at the reference temperature.

The PV energy equation is solved numerically like glass energy equation.

For the absorber plate, it receives heat from the PV plate and transferred to both the tube and insulation. Therefore, the energy equation is written as:

$$\rho_{ab}\delta_{ab}C_{ab}\frac{dT_{ab}}{dt} = U_{cond,pv\to ab}(T_{pv}-T_{ab}) - \frac{A_{ab,t}}{A_{ab}}U_{cond,ab\to t}(T_{ab}-T_t) - \frac{A_{ab,in}}{A_{ab}}U_{cond,ab\to in}(T_{ab}-T_{in}) + \delta_{ab}\nabla.(k_{ab}\nabla T_{ab}) \quad (14)$$

where A_{ab} is the computational cell surface area of the absorber and subscript ab refers to the absorber plate; $U_{cond,ab\to t}$ and $U_{cond,ab\to in}$ are the absorber total heat transfer coefficient to the wall tube and the insulation, respectively, calculated similarly as of Eq. (11). $A_{ab,t}$ and $A_{ab,in}$ are contact area of computational cell with the tube, and the insulation respectively.

The absorber energy equation (Eq. (14)) along with its boundary conditions is solved numerically using the same procedure as explained for the glass plate energy equation (Eq. (7)).

For the tube wall, the heat it receives from the absorber plate is transferred to both the fluid and the insulation. Therefore, the energy equation for the tube wall is written as:

$$\rho_t\delta_t C_t P dx\frac{dT_t}{dt} = A_{ab,t}U_{cond,ab\to t}(T_{ab}-T_t) + A_{in,t}U_{cond,t\to in}(T_{in}-T_t) + h_{conv,t\to f}Pdx(T_f-T_t) + k_t\delta_t Pdx\frac{\partial^2 T_t}{\partial x^2} \quad (15)$$

where subscript t refers to the tube wall; $U_{cond,t\to in}$ and $h_{conv,t\to f}$ are the total heat transfer coefficient between the insulation and tube wall calculated similarly as of Eq. (11) and convection heat transfer coefficient to the fluid respectively. $A_{in,t}$ is the interfacial area of the control volume between the tube wall and the insulation. This control volume is a ring around the tube with a lateral area of Pdx.

For the fluid, it receives heat from the tube wall. Therefore, the energy equation is written as:

$$\rho_f A_f C_f dx\frac{dT_f}{dt} = h_{conv,t\to f}Pdx(T_t-T_f) - \dot{m}C_f dx\frac{\partial T_f}{\partial x} + \frac{\partial}{\partial x}\left(k_f A_f\frac{\partial T_f}{\partial x}\right)dx \quad (16)$$

where subscript f refers to the fluid and A_f is the cross sectional area of fluid.

The numerical procedure for solving the tube wall and fluid energy equations (Eqs. (15) and (16)) is the same as that of the previous equations (Eqs. 7, 12 and 14).

The calculation procedure of the convection heat transfer coefficient between tube wall and the fluid is given later in this section.

Because of low thermal conductivity of insulation, it is assumed that all contact area are insulation and do not have any conduction. So $U_{cond,ab\to in}$ and $U_{cond,t\to in}$ are equal to zero.

Side walls of the glass, PV, and absorber plates have convection heat transfer to the ambient. The PV and Glass plates receive radiation from the Sun. The upper surface of the glass plate have convection to the ambient. The boundary condition at the tube inlet is a known fluid temperature (T_i). At the tube outlet, the gradient of fluid temperature is assumed to be zero (Fig.2c). A fixed mass flow rate of the fluid is considered for the entire experiments in this paper.

Convection heat transfer inside the tube. The convection heat transfer between fluid and the tube wall is based on an analytical method as given below. From the definition of the Nusselt number (Nu), we have:

$$h_{conv,f\to t} = \frac{Nu_{nf}k_{nf}}{d_t} \quad (17)$$

where subscript nf is the nanofluid, d_t is the inner diameter of the tube and Nu is the Nusselt Number defined as the ratio of convection to conduction heat transfer in a fluid flow. Since the flow in all experiments are laminar ($Re_{nf} < 3000$) the Nusselt number in the circular tube is calculated using [27]:

$$Nu_{nf} = 4.36 + \frac{0.086\left(\frac{Re_{nf}Pr_{nf}d_t}{L_t}\right)^{1.33}}{1 + Pr_{nf}\left(\frac{Re_{nf}d_t}{L_t}\right)^{0.83}} \quad (18)$$

where L_t refers to length of tube. Re and Pr are the Reynolds and Prandtl numbers for the nanofluid calculated as [28]:

$$Re_{nf} = \frac{4\dot{m}_{nf}}{\pi d_t\mu_{nf}} \quad (19)$$

$$Pr_{nf} = \frac{\mu_{nf}C_{nf}}{k_{nf}} \quad (20)$$

where $\dot{m}_{nf}$ is the fluid mass flow rate. The Reynolds number is a dimensionless number defined as the ratio of inertial forces to viscous forces in a flowing fluid and the Prandtl Number is a dimensionless number approximating the ratio of momentum diffusivity (kinematic viscosity) to thermal diffusivity.

In this section in order to simulate the PVT system by FORTRAN, energy equations are solved for the entire plates and the tube flow using an implicit formulation and the TDMA numerical method. The plates include: glass cover, PV plate and absorber plate. The tube wall and the fluid flow inside the tube are also included in the simulations. The thermo-physical properties for the fluid are assumed to be temperature dependent.

3.4. Exergy and entropy generation

The first law of thermodynamics only indicates the conservation of energy; it does not show the quality of the energy. The thermal and electrical efficiencies based on this law are given as:

$$\eta_{th} = \frac{\dot{E}''_{th}}{\dot{E}''_{in}} \quad (21)$$

$$\eta_{el} = \frac{\dot{E}''_{el}}{\dot{E}''_{in}} \quad (22)$$

where $\dot{E}''_{in}$, $\dot{E}''_{th}$ and $\dot{E}''_{el}$ refer to energy rate of input, thermal and electrical per unit area, respectively.

Exergy represents the maximum quantity of work that can be produced in some given environment. By considering the PV unit and the thermal collector as a combined control volume and assuming a transient condition, the exergy balance can be expressed as:

$$\dot{E}x''_{in} = \dot{E}x''_{th}. + \dot{E}x''_{el}. + \dot{E}x''_{loss}. \quad (23)$$

where $\dot{E}x''_{.in}$, $\dot{E}x''_{.th}$, $\dot{E}x''_{.el}$ and $\dot{E}x''_{.loss}$ refer to exergy rate of input, thermal, electrical and losses per unit area, respectively. The exergy efficiency of the PVT has two parts namely electrical and thermal exergy efficiencies defined as [2]:

$$\eta_{II,th} = \frac{\dot{E}x''_{th}}{\dot{E}x''_{in}} \tag{24}$$

$$\eta_{II,el} = \frac{\dot{E}x''_{el}}{\dot{E}x''_{in}} \tag{25}$$

where $\eta_{II,th}$ and $\eta_{II,el}$ are thermal and electrical exergy efficiencies, respectively. The thermal energy and exergy rates per unit area are calculated using the following [16]:

$$\dot{E}''_{th} = \frac{\dot{m}_{nf} C_{nf} (T_o - T_i)}{A} \tag{26}$$

$$\dot{E}x''_{th} = \dot{E}''_{th} - \frac{\dot{m}_{nf} c_{nf} T_{amb} \ln\left(\frac{T_o}{T_i}\right)}{A} \tag{27}$$

where T_o and T_i are the fluid outlet and inlet temperatures, respectively, and A is the tube cross sectional area.

The total obtained electrical energy from a PVT system is considered an available energy; therefore, the electrical exergy rate is equal to that of the energy rate [2]:

$$\dot{E}x''_{el} = \dot{E}''_{el} \tag{28}$$

The input energy per unit area from the sun is the amount of irradiation absorbed by the PV cells calculated based on [2]:

$$\dot{E}''_{in} = \alpha_{pv} \tau_g G \tag{29}$$

The input exergy rate per unit area is also calculated from the following [10]:

$$\dot{E}x''_{in} = G\left(1 - \frac{4T_{amb}}{3T_{sun}} + \frac{1}{3}\left(\frac{T_{amb}}{T_{sun}}\right)^4\right) \tag{30}$$

where T_{sun} is the sun surface temperature (as a black body $T_{sun} \cong 5800\,\mathrm{K}$) [2].

The entropy generation of fluid flow in a circular tube is due to both thermal and frictional losses. The thermal entropy generation per unit volume is relevant to temperature gradient as [29]:

$$\dot{S}'''_{gen,thermal} = \frac{k_{nf}}{T_{amb}^2}\left[\left(\frac{\partial T}{\partial r}\right)^2 + \left(\frac{1}{r}\frac{\partial T}{\partial \theta}\right)^2 + \left(\frac{\partial T}{\partial z}\right)^2\right] \tag{31}$$

The frictional entropy generation is related to the pressure drop which is increased by increasing viscosity or flow velocity. The pressure drop can be obtained as [30]:

$$h_f = \frac{128 \dot{m}_{nf} \mu_{nf} L}{\pi d_t^4 \rho_{nf}^2 g} \tag{32}$$

$$\sum h_m = \frac{V^2}{2g} \sum K$$

$$\Delta P = \rho_{nf} g (h_f + \sum h_m)$$

where h_f, h_m and K are the frictional head loss of the tube, the minor loss (due to the pipe entrance, exit and bends), and the loss coefficient, respectively. The frictional entropy generation is then calculated based on the following [31]:

$$\dot{S}_{gen,frictional} = \frac{\dot{m}_{nf} \Delta P \ln\left(\frac{T_o}{T_i}\right)}{\rho_{nf} (T_o - T_i)} \tag{33}$$

By subtracting the exergy of the output from that of the input and using Eq. (23), the total exergy loss of the system can be obtained. The rate of total entropy generation of the system, is then calculated by dividing the total exergy loss to the ambient temperature for the selected control volume as [32]:

Table 4
The grid study.

Dimensions	63 × 54	76 × 65	88 × 76	101 × 86	126 × 108
Outlet Temperature (K)	316.94	316.79	316.85	316.87	316.88
Computation Time (s)	98	121	192	242	489

$$\dot{S}''_{\cdot gen,system} = \frac{\dot{E}x_{\cdot loss}}{T_{amb}} \tag{34}$$

3.5. Grid study

As mentioned earlier, a 2D model is used to simulate heat transfer in the plates. According to Fig. 2, due to their small thicknesses, all plates are assumed to have a thickness of one cell and are discretized in x and y directions. For the tube and fluid flow, the heat transfer problem is assumed to be radially lumped; as a result, the discretization is performed only in the axial direction. The contact area between the tube and the absorber plate is assumed to be one eighth of the total tube lateral area.

Table 4 shows that the outlet temperature is almost same in all considered grids; therefore, a grid size of 101 × 86 is selected in the present study.

4. Result and discussion

The results of this study are provided in three sections. First, the numerical data are validated with those of the experiments for various cases, after which the variation of mass fraction on the PVT performance is studied while other conditions are kept constant. Next, the thermo-physical properties of different nanofluids versus the mass fraction are investigated. Based on Table 2, the nanofluid properties depend on the mean temperature distribution; therefore, to determine the properties in each mass fraction, the temperature distribution is found numerically. Finally, having obtained the fluid properties, the energy, exergy and entropy analyses at various mass fractions are performed.

4.1. Validation

The numerical results are validated by a comparison of the temperature of the PV plate and that of the liquid outlet with those of the experiments. The comparison is performed for different nanofluidsAl_2O_3/water, TiO_2/water and ZnO/water by 0.2 wt%, and SiO_2/water by 1 wt% and 3 wt%. The temperatures in the experiments are measured each 30 min from 9:30 to 15:30 local time, in the outdoor weather condition. Solar radiation rate (per unit area), fluid inlet and the ambient temperatures, from the experiments, are used as the inputs for the numerical model.

Fig. 3a and 3 b display the comparison of the fluid outlet temperatures calculated from the model with those of the experiments for various nanofluids. A good agreement is observed between the results of simulations and measurements with average errors of 2.19%, 2.10%, 1.63%, 1.95% and 1.63% for nanofluids Al_2O_3/water, ZnO/water and TiO_2/water by 0.2 wt%, and SiO_2/water by 1 wt% and 3 wt% respectively. The small discrepancies between the two results may be attributed due to the simplifying assumptions in the numerical model and the uncertainties of measuring instruments in the experiments.

Fig. 4a and 4 b show the comparison of the surface temperature of PV plate from experiments and numerical simulations during the day for studied nanofluids in this paper. The comparison of simulations and measurements shows average errors of 2.85%, 2.05%, 2.08%, 2.61% and 2.99% for nanofluidsAl_2O_3/water, ZnO/water and TiO_2/water by 0.2 wt%, and SiO_2 /water by 1 wt% and 3 wt%, respectively. The small discrepancies between the two results for surface temperatures from

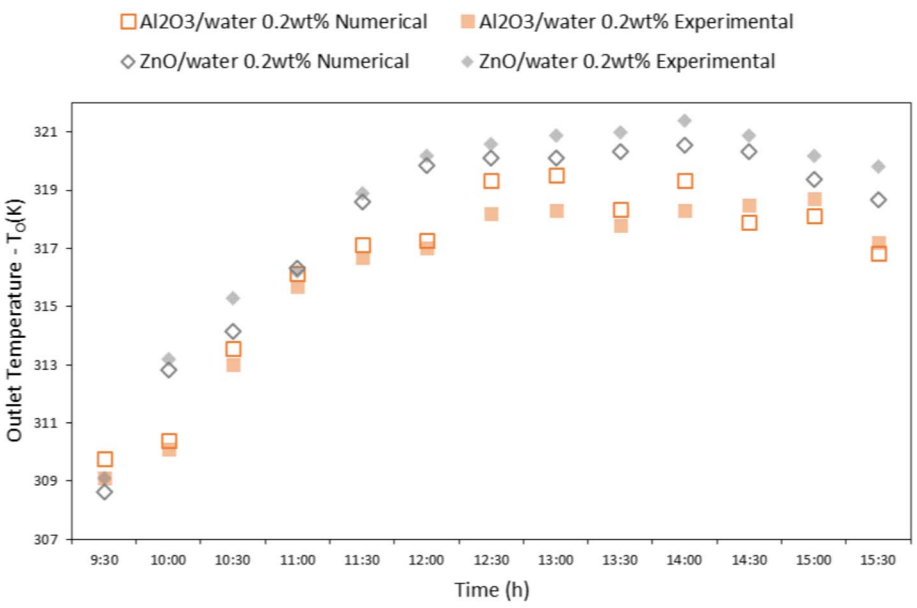

Fig. 3. The numerical and experimental value of the fluid outlet temperature during the day for all studied nanofluid (a) Al_2O_3/water and ZnO/water by 0.2 wt% (b) TiO_2/water by 0.2 wt% and SiO_2/water by 1 wt% and 3 wt%.

experiments and simulations may be attributed to the simplifying assumptions in the numerical model and the uncertainties of measuring instruments in the experiments.

In this section, the numerical results were validated with experimental data of the PV surface and fluid outlet temperatures.

4.2. Thermo-physical properties

Adding nanoparticles changes thermo-physical properties of the nanofluid which affect various efficiencies of the PVT system from both energy and exergy viewpoints.

For a constant mass flow rate of the nanofluid, adding nanoparticles increases its density and viscosity as displayed in Fig. 5.

From Fig. 5, a relatively large difference is observed between the values of density and viscosity for SiO_2/water nanofluid compared to those of other nanofluids. The volume fraction of SiO_2/water is greater than that of other nanofluids in the same mass fraction which is due to the low density of SiO_2 nanoparticle in comparison with the density of other nanoparticles. This may be considered to be main reason for the high viscosity of SiO_2/water nanofluid (see Eq. (5)).

The Reynolds number versus mass fraction for various nanofluids are presented in Fig. 6. As observed, Reynolds number is decreased by adding nanoparticles to the base-fluid due to an increase of viscosity (Fig. 6 and Eq. (19)). Therefore, adding nanoparticles make the fluid flow more laminar.

From Fig. 6, the Reynolds number for the SiO_2/water nanofluid is less than that of the other nanofluids. For the ZnO/water nanofluid by increasing the mass fraction, a less increase of the viscosity is observed compared to that of the other nanofluids (Fig. 5b).

Another important property of the nanofluid is the specific heat capacity that can significantly affect the efficiency of the system. Fig. 7 displays the variation of specific heat versus mass fraction for different nanofluids. As the specific heat of base-fluid (water) is much more than that of the nanoparticles (around 4200 J/kg K for water compared to

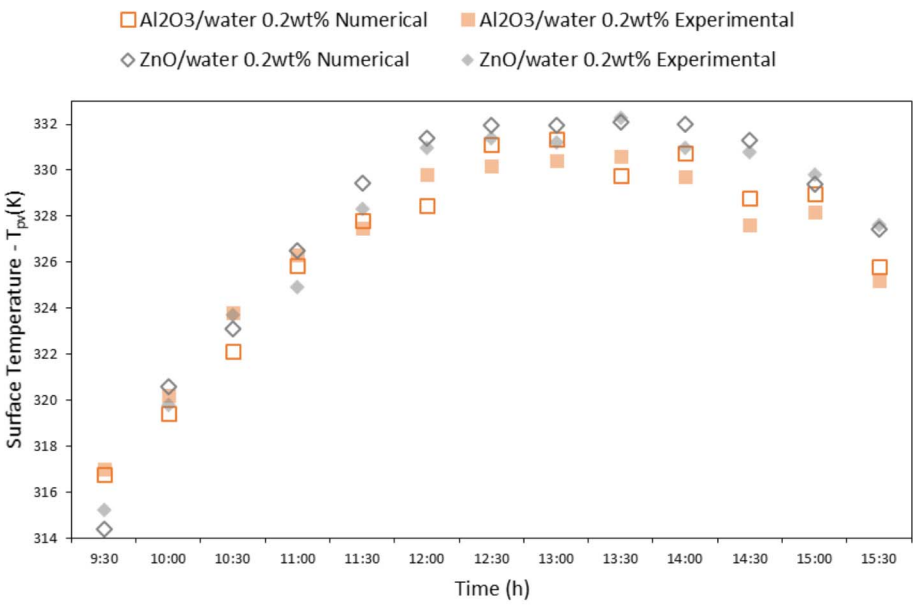

Fig. 4. The numerical and experimental value of the surface temperature during the day for all studied nanofluid (a) Al_2O_3/water and ZnO/water by 0.2 wt% (b) TiO_2/water by 0.2 wt% and SiO_2/water by 1 wt% and 3 wt%.

values of less than 800 J/kg K for nanoparticles given in Table 3), increasing the mass fraction of nanoparticles in the nanofluid will decrease its specific heat. Based on Fig. 7, for almost all nanofluids, the variation of specific heat with mass fraction is similar which is due to that, their specific heat values of their corresponding nanoparticles are in same range compare to water.

The thermal conductivity is one of the important parameters of the heat transfer coefficient of the working fluid.

Based on Fig. 8, it is seen that by increasing the nanofluid mass fraction, Al_2O_3/water has the most thermal conductivity and SiO_2/water has the lowest in the same mass fraction. For a specific mass fraction, the nanoparticle density and thermal conductivity as well as the nanofluid mean temperature can affect the thermal conductivity of nanofluids. The highest thermal conductivity of Al_2O_3/water nanofluid can be the result of higher value of Al_2O_3 thermal conductivity compared to that of the other nanoparticles.

Fig. 9 displays the variation of the Prandtl number versus mass fraction of various nanofluids.

It can be seen from the figure that, while for metallic nanofluids such as: Al_2O_3, ZnO, and TiO_2/water by increasing the mass fraction of the nanoparticles, the Prandtl number is decreased, for metalloid nanofluids such as SiO_2/water, the Prandtl number remains nearly constant. This can be attributed to the higher thermal diffusivity of metallic nanofluids compared to the lower thermal diffusivity of SiO_2/water nanofluid (based on Figs. 8 and 5b and Eq. (20)).

This section showed the variation of thermo-physical properties and Reynolds and Prandtl numbers by changing the mass fraction of different nanofluids. It is found that adding nanoparticle can improve the thermo-physical properties of coolant fluid.

4.3. Heat transfer

The heat transfer coefficient between the coolant nanofluid and the tube wall is investigated in this section.

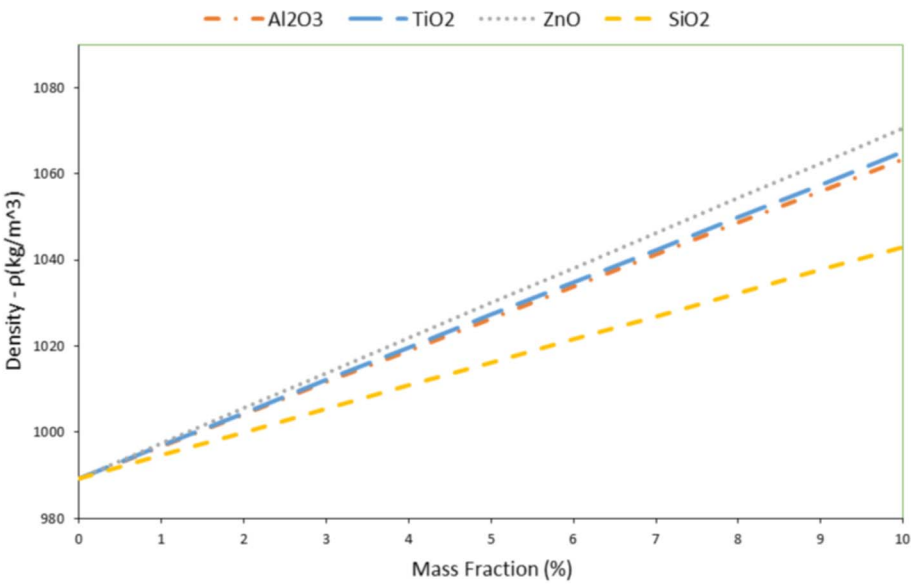

(a)

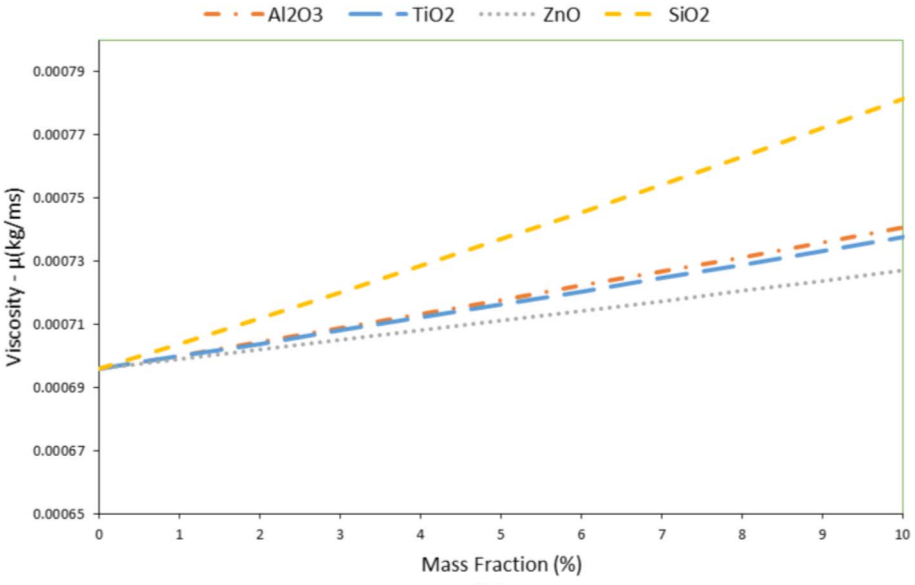

(b)

Fig. 5. a) density and b) viscosity of the studied water-based nanofluids versus mass fraction.

Adding nanoparticles increases the thermal conductivity and density of the nanofluid which are favorable parameters in the heat transfer. While, the viscosity of the nanofluid is increased and the specific heat capacity is decreased which are unfavorable parameters in heat transfer coefficient. It is well known, however, that the most effective parameter on heat transfer coefficient is thermal conductivity [33].

Based on Fig. 10, the metalloid nanofluid (SiO_2/water) has the lowest heat transfer coefficient in the same mass fraction, due to its unfavorable parameter such as high viscosity and low thermal conductivity of it compared to other studied nanofluids.

The Nusselt number is considered as a function of Reynolds and Prandtl numbers. For a laminar flow with constant mass flow rate, increasing the nanoparticles decreases the Reynolds and Prandtl numbers, therefore, based on Eq. (18), it can be seen that by increasing the mass fraction, the Nusselt is decreased (Fig. 11). By increasing the mass fraction in different nanofluids, the thermal conductivity is increased, which in turn, reduces the Nusslet number. In this study, it is found that the Nusselt Number is not a good criterion for predicting the heat transfer; instead the heat transfer coefficient should be used [31].

This section showed the effect of adding nanoparticle on heat transfer coefficient and Nusselt number. It is observed that adding nanoparticle can improve the heat transfer in PVT systems.

4.4. Thermodynamics analysis

To calculate the thermal and frictional entropy generations, the temperature distribution in all plates and in the working fluid and the pressure drop must be determined which can be easily obtained from the numerical model.

As given in the mathematical model section, the fluid outlet temperature has an important role on the thermal efficiencies based on the 1st and 2nd laws of thermodynamics.

The outlet temperature ratio vs. mass fraction for four different nanofluids is presented in Fig. 12. As observed by increasing the mass fraction of nanofluid, the outlet temperature is increased.

The first law of thermodynamics shows the energy balance of the system. The numerical results based on this law show that by increasing

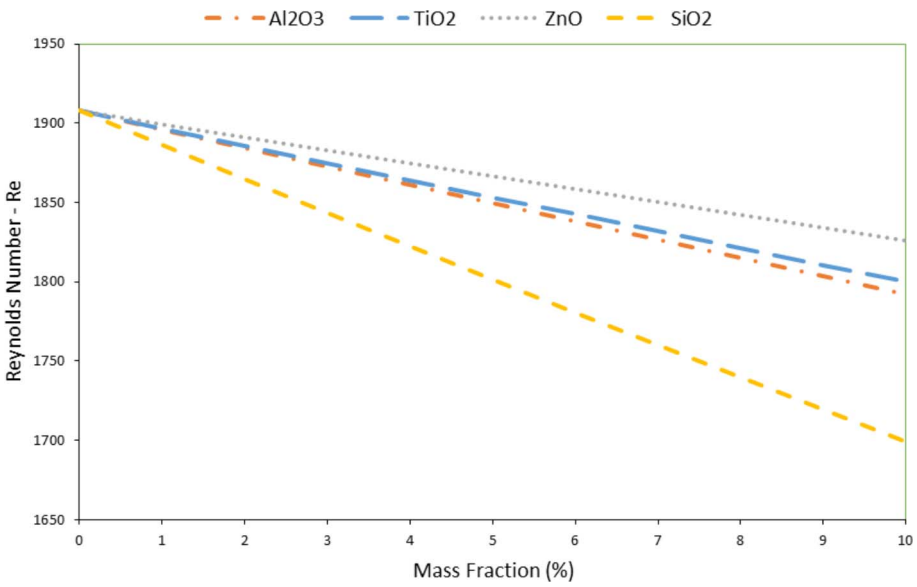

Fig. 6. Reynolds number of the studied water-based nanofluids versus mass fraction.

nanofluid mass fraction, thermal and electrical efficiencies are increasing. According to Eqs. (13) and (22), the electrical efficiency is directly related to the surface temperature. Adding nanoparticles increase the electrical efficiency by reducing the surface temperature. Increasing mass fraction of nanofluids in a PVT system does not change the surface temperature considerably compared to that PVT system with pure water. Therefore, increasing mass fraction has a negligible effect on the electrical efficiency. According to Eqs. (21) and (26), the thermal efficiency (in a constant mass flow rate) is affected by the specific heat capacity and the fluid outlet temperature. The numerical results show that there is 6.23%, 6.02%, 6.88% and 5.77% increase in thermal efficiency of Al_2O_3, TiO_2, ZnO and SiO_2/water nanofluids by 10 wt% compared those of the pure water. Furthermore, by comparing Fig. 11 and Fig. 12, it is found that the trend of Nusselt number and outlet temperature variations are completely opposite. Therefore, it may be concluded that by increasing the Nusselt number, the outlet temperature can be minimized.

The performance of the system cannot be evaluated based on the energy analysis alone, because it does not consider the process direction, the energy quality and irreversibilities. Therefore, in order to investigate the performance of PVT systems, an exergy analysis is necessary [34,35]. It should be noted that the exergy of PVT systems can be determined from two viewpoints, net output exergy and entropy generation [35,36].

In a PVT system, the heat is absorbed by the collector, therefore, based on the 1st law of thermodynamic, it will increase the energy efficiency of system. Based on the 2nd law, all processes include irreversibilities that must be considered as well. Therefore, the system analysis should be performed using both the 1st and 2nd laws. Based on the energetic viewpoint, the thermal efficiency is greater than that of the electrical, while in the exergy viewpoint it is vice versa.

It is found in this research that the electrical exergy efficiency of the PVT system remains nearly constant for various nanofluids (the enhancement of electrical exergy efficiency is 1.18%, 1.16%, 1.23% and 1.11% for Al_2O_3, TiO_2, ZnO and SiO_2/water nanofluids by 10 wt% compared to those of pure water, respectively). The thermal exergy efficiency, however, is enhanced by increasing the mass fraction of nanofluids as seen in Fig. 13, the enhancement of thermal exergy efficiency is 10.11%, 10.08%, 10.39% and 9.94% for Al_2O_3, TiO_2, ZnO and SiO_2 /water nanofluids by 10 wt% compared to those of the pure water, respectively. Based on Eq. (27), the specific heat capacity and fluid outlet temperature can have an effect on the thermal exergy. In this

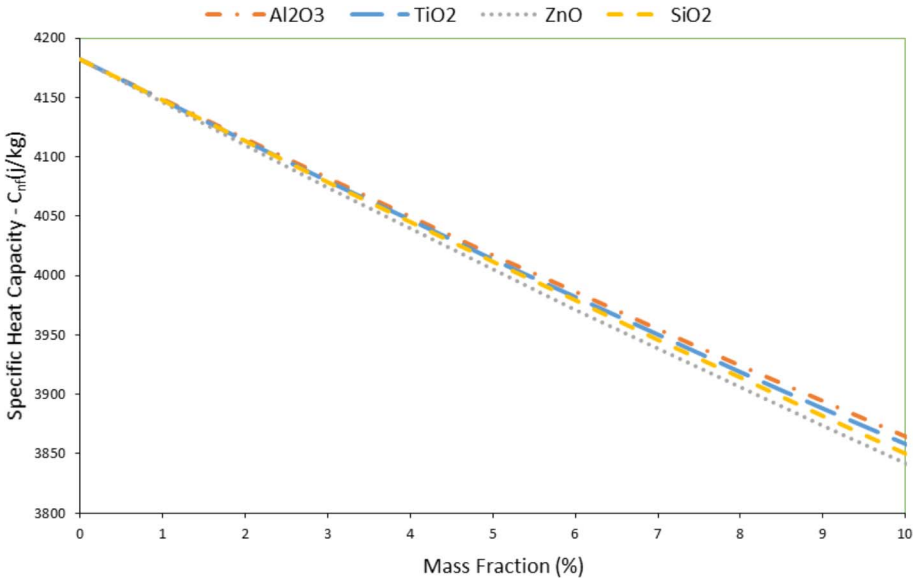

Fig. 7. Specific heat capacity of the studied water-based nanofluids versus mass fraction.

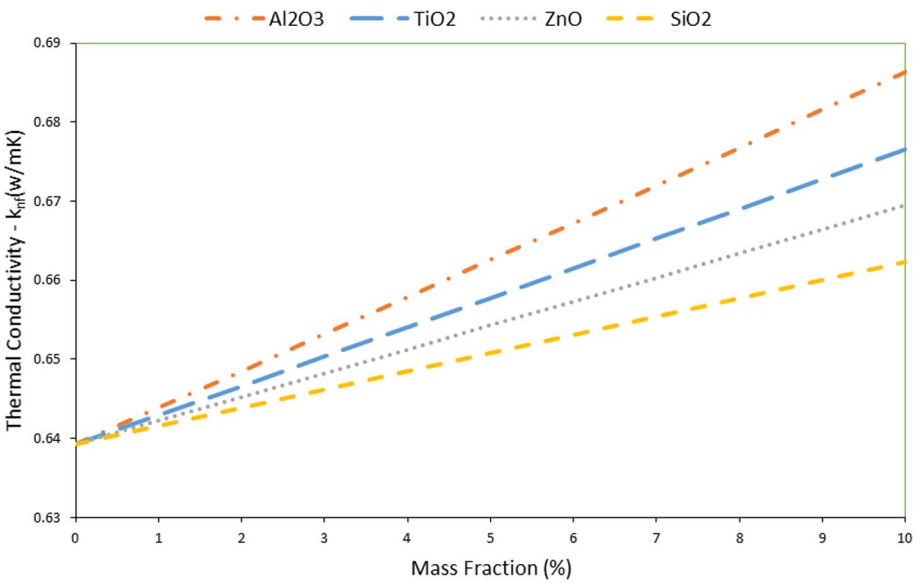

Fig. 8. Thermal conductivity of the studied water-based nanofluids versus mass fraction.

study, the outlet temperature of ZnO /water is found to be more than that of the other nanofluids while the specific heat capacity remains almost constant for all nanofluids at the same mass fraction. Thus, it can be concluded that ZnO /water nanofluid has the maximum thermal exergy efficiency (as seen in Fig. 13). It is found that the total exergy of the PVT system for pure water, Al_2O_3,TiO_2, ZnO and SiO_2 /water nanofluids by 10 wt% are 13.71%, 14.98%, 14.72%, 15.05%, 14.53% respectively. It is found that ZnO /water has the highest total exergy compared to other nanofluids.

In this section, the effect of adding nanoparticle on efficiencies based on 1st and 2nd laws of thermodynamics were investigated. It is showed that adding nanoparticle can improve the efficiencies in PVT systems.

4.5. Cost analysis

Bhattarai et al. [37] compared photovoltaic and thermal solar water based collector. They concluded that the cost pay back period of the PVT system is lower than that of the PV module and higher than the conventional solar thermal collector. Faizal et al. [38] found that by using nanofluid as coolant in solar collector, large portion of copper and glass used in the system can be eliminated based on the scaling of the overall percentage weight of the collector. The capital cost of the collector will then be offset by the cost of nanoparticles. The economic aspects of using nanofluids in the PVT systems are rare and the cost can vary by local energy cost and government subsidies [39].

The economic analysis performed in this study is based on following assumptions:

- Electrical consumption of circulating pumps are considered;
- Cost of nanofluids is taken into account;
- Annual maintenance cost is assumed to be 2% of the initial cost;
- Annual interest rate of the initial cost and cumulative saving is assumed to be 2%;
- Systems are assumed to continuous produce electricity (i.e., connected to the grid).

The electricity cost charged to residental users is currently around 0.06 US $/kWh which is expected to be increased up to the finished cost (around 0.29 US $/kWh) by March 2018 [39].

Agustin et al. [40] expressed an equation for the initial cost of the electricity generation, by considering the generator, inverter,

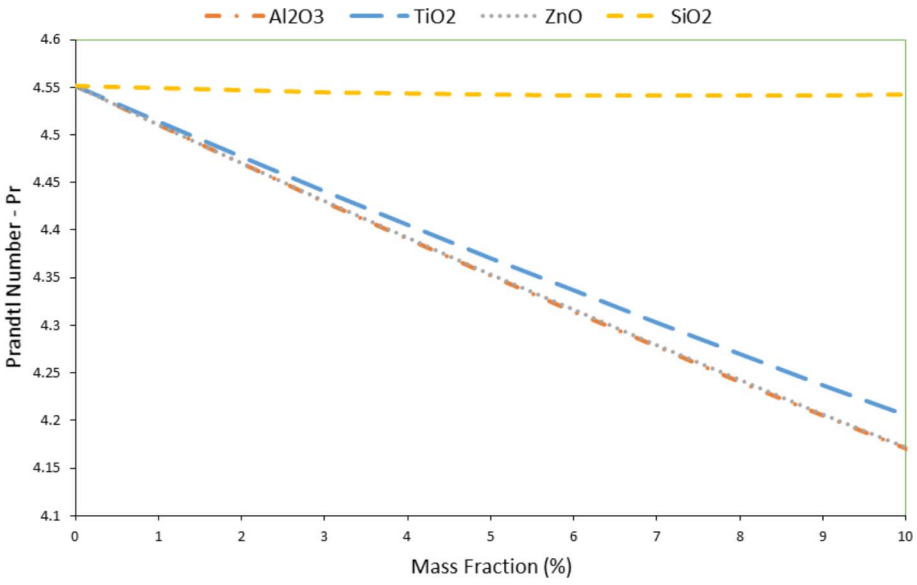

Fig. 9. Prandtl number of the studied water-based nanofluids versus mass fraction.

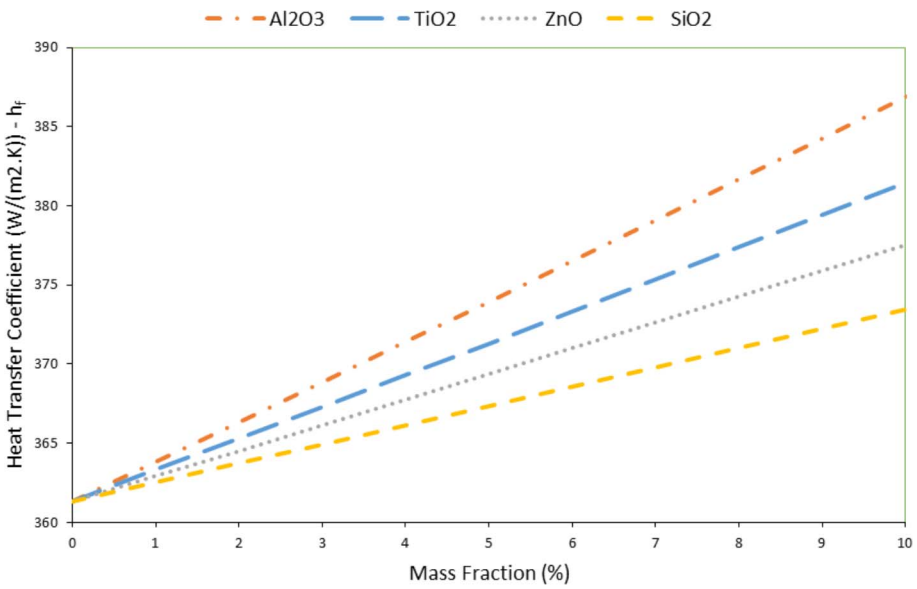

Fig. 10. the heat transfer coefficient of Al_2O_3/water, TiO_2/water, ZnO/water and SiO_2/water versus mass fraction.

installation and subsidy costs.

$$C_{total} = C_{gen} + C_{inst} + C_{inv} - C_{sub} \quad (35)$$

where C indicates the item cost and subscripts *gen*, *inst*, *inv* and *sub* refer to power generators (PV or PVT), installation, inverter and subsidy.

In this study, in addition to the above mentioned costs, the pump and nanofluid costs (C_{nano} *and* C_{pump}) are also considered. Therefore, Eq. (35) can be rewritten as:

$$C_{total} = C_{gen} + C_{pump} + C_{inv} + C_{np} + C_{ins} - C_{sub} \quad (36)$$

Based on the economic analysis, payback period is calculated for the system. The results of the paybackperiod calculations can be seen in Fig. 14.

This section showed the economic aspects of using nanofluid in the PVT systems. It is observed that adding nanoparticle can reduce the long-term cost of energy in PVT systems.

4.6. Entropy generation

Maximizing the power output of a system, is similar to minimizing the entropy generation. The entropy generation is a proper parameter to show the system irreversibilities. In this research, the effect of different nanofluids mass fraction on three types of entropy generation is studied.

First, the fluid thermal entropy generation is calculated locally to show the thermal irreversibility of the coolant fluid (entropy generation due to heat transfer). Second, the fluid frictional entropy generation that shows the irreversibility of fluid due to friction (i.e., the pressure drop), is investigated. Finally, the system total entropy generation is calculated that shows the total irreversibilities of the system.

Based on Eq. (32), since the mass flow rate is constant, two main parameters that affect the pressure drop are the velocity and viscosity of the nanofluid.

Fig.15a shows the pressure drop ratio in the tube. According to this figure, metallic nanofluids can decrease the pressure drop that has an effect on pumping power which is favorable. Also, it is found that the metalloid nanofluid (SiO_2/water) can increase the pressure drop which is undesirable.

For metallic nanofluids, increasing nanoparticle mass fraction results in an increase of the nanofluid density (Fig. 5a), which in turn, in a constant mass flow rate reduces the velocity and also by increasing mass fraction the fluid outlet temperature will increase which lead to a

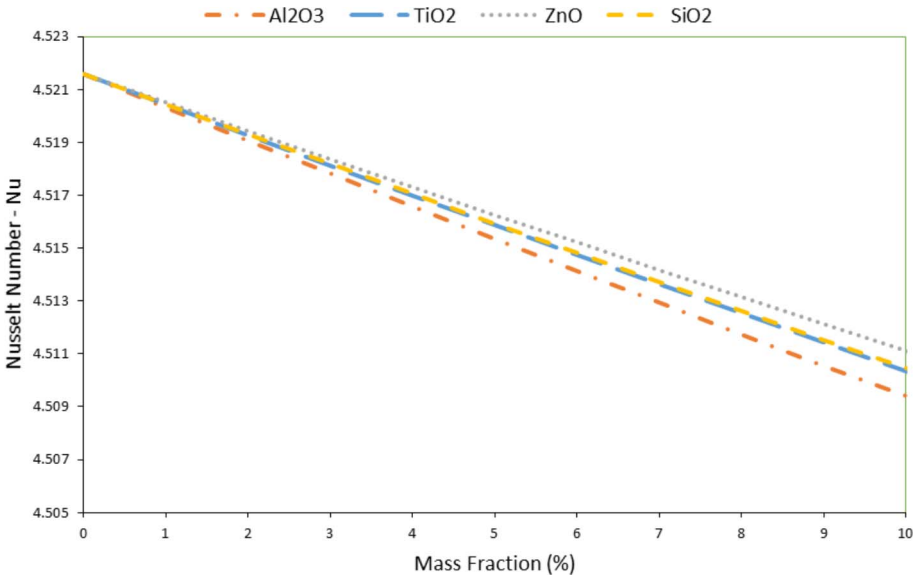

Fig. 11. The Nusselt number of Al2O3/water, TiO2/water, ZnO/water and SiO2/water versus mass fraction.

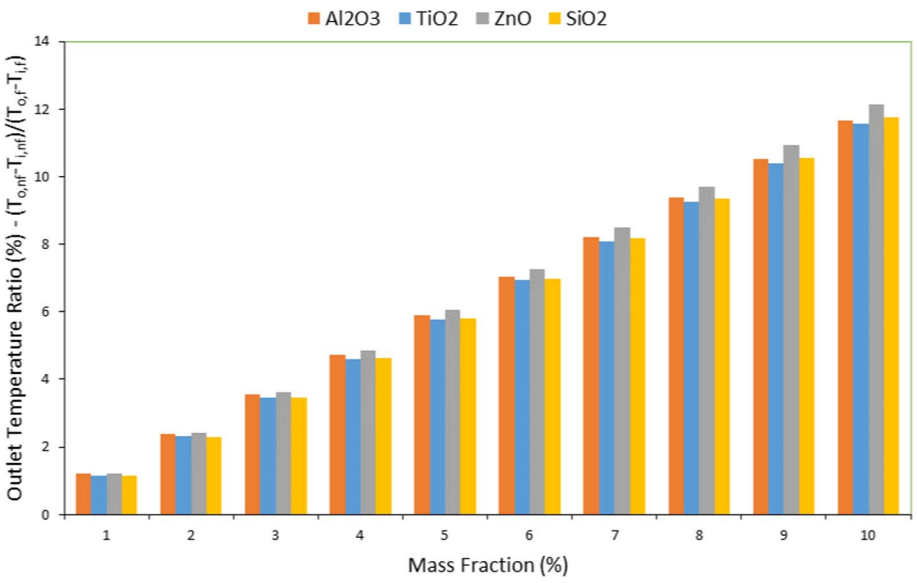

Fig. 12. The fluid outlet temperature ratio of Al_2O_3/water, TiO_2/water, ZnO/water and SiO_2/water to the pure water versus mass fraction.

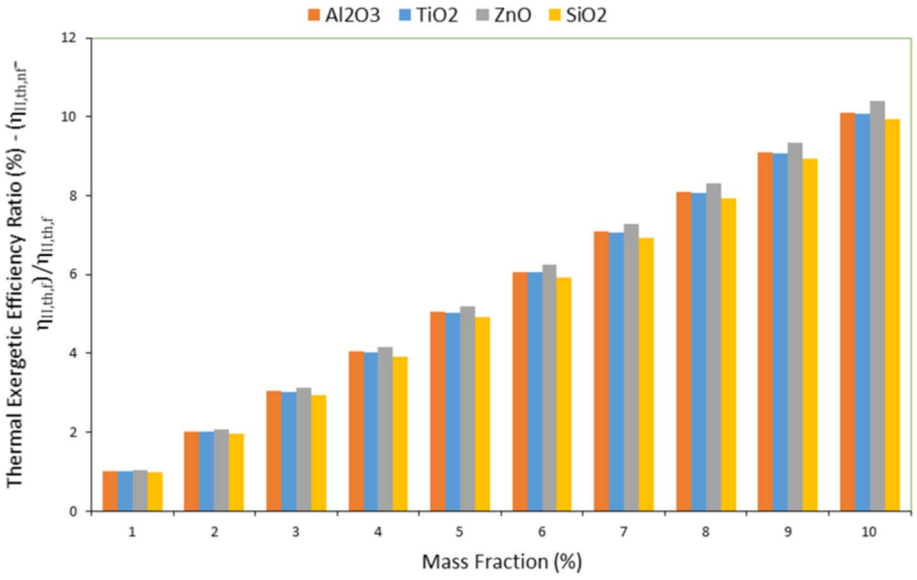

Fig. 13. The thermal exergetic efficiency ratio of Al_2O_3/water, TiO_2/water, ZnO/water and SiO_2/water to the pure water versus mass fraction.

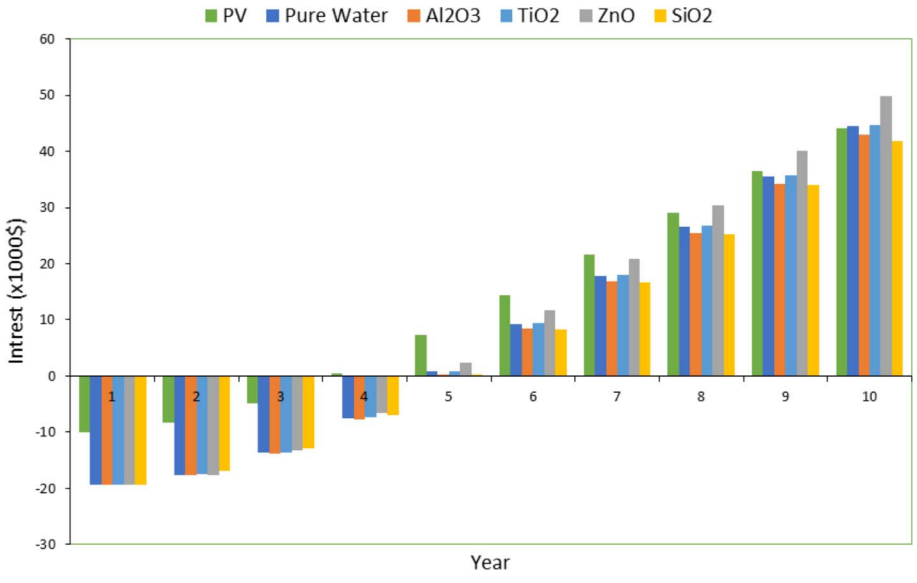

Fig. 14. Payback period diagram of a 1 kW PVT system from the energy viewpoint.

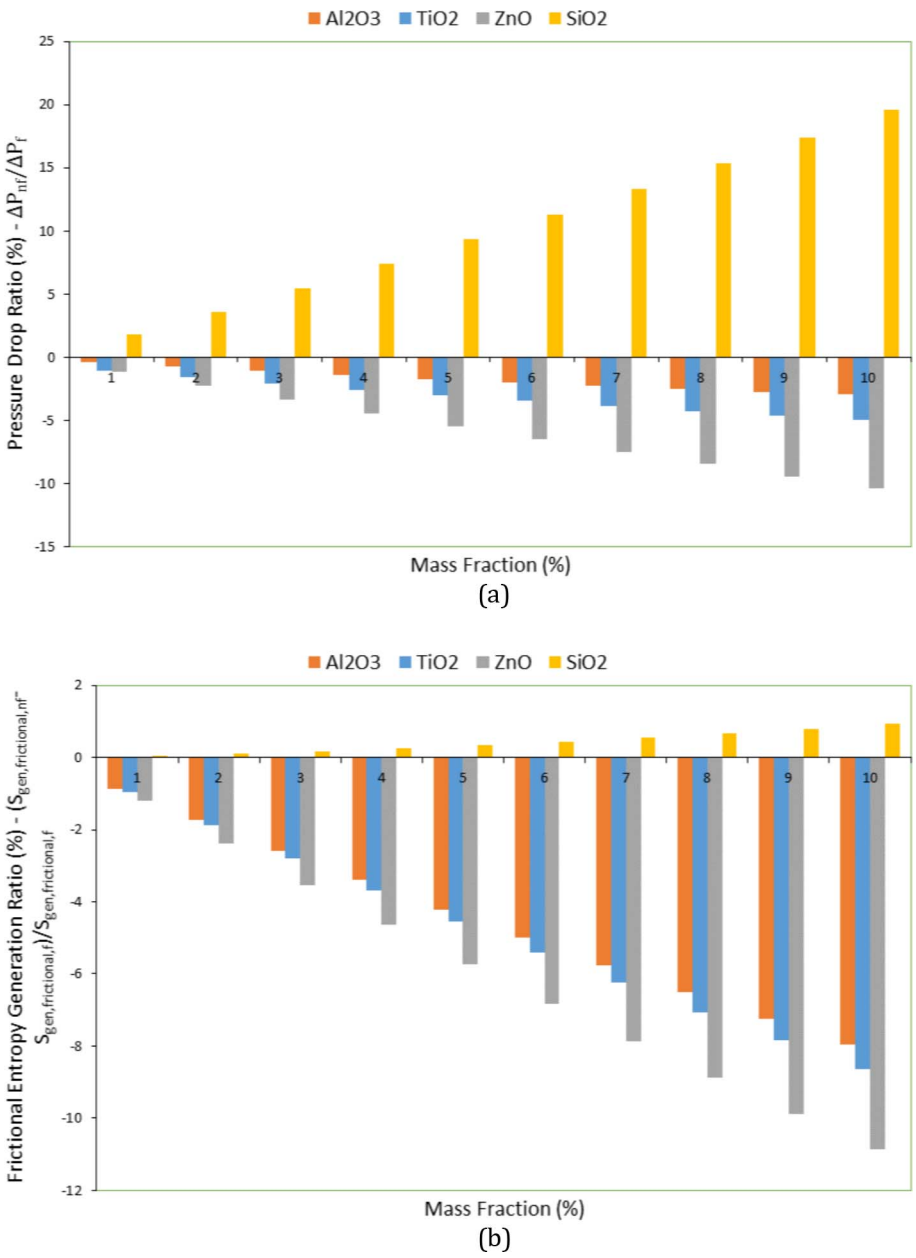

Fig. 15. (a) Pressure Drop and (b) The frictional entropy generation ratio of Al_2O_3/water, TiO_2/water, ZnO/water and SiO_2/water to the pure water versus mass fraction.

decrease of the frictional entropy generation (see Fig. 15b and Eqs. (32) and (33)). On the other hand, by increasing mass fraction, the viscosity of nanofluid is increased that has a reverse effect on the frictional entropy generation. However, based on Fig. 15b, by increasing mass fraction metallic entropy generation will be reduce. It was found that for ZnO/water nanofluid, the least frictional entropy was generated.

For metalloid nanofluid (SiO_2/water in this study) at a same mass fraction, the pressure drop and frictional entropy generation are more than those of the other nanofluids considered in this paper (see Fig. 15). This is because of higher viscosity and velocity of SiO_2 /water compared to other nanofluids.

The thermal entropy generation for the entire cases is presented in Fig. 16. It can be seen that by increasing mass fraction, the thermal entropy generation in all nanofluids will decrease. Al_2O_3/water has the best performance among other nanofluids due to its high heat transfer coefficient as mentioned above. The thermal entropy generation for Al_2O_3/water is reduced by 6.24% at 10 wt% compared to that of pure water.

The thermal entropy generation distribution in the collector is given in Fig. 17. According to this figure, fluid thermal entropy generation is increased at the entrance and at the tube turning points and also in the last row close to the exit. This is because of a higher temperature difference between the tube connected to the absorber plate and the fluid at those locations.

The total entropy generation is due to exergy loss of the total PVT system. It is found that, by increasing the mass fraction of nanofluid, the total system entropy generation will be reduced. Al_2O_3/water has the best and SiO_2/water has the worst performance with respect to total entropy generation among nanofluids considered in this study. It is found that the change of the thermal entropy generation is higher than that of the frictional entropy generation.

In this section, the effect of adding nanoparticle on the thermal and frictional entropy generations were investigated. The results showed that metallic nanofluids decreased the entropy generation more than metalloid nanofluid in PVT systems.

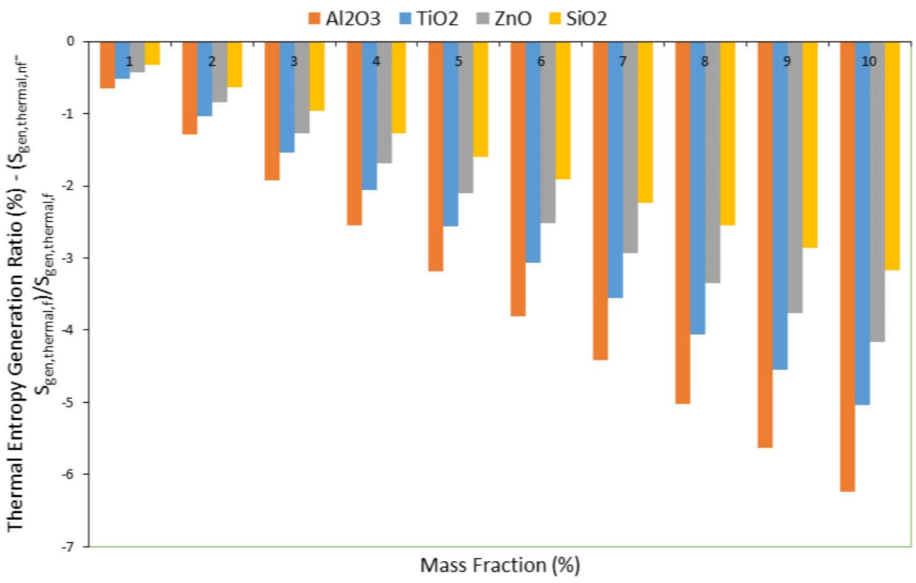

Fig. 16. The thermal entropy generation ratio of Al_2O_3/water, TiO2/water, ZnO/water and SiO_2/water to the pure water versus mass fraction.

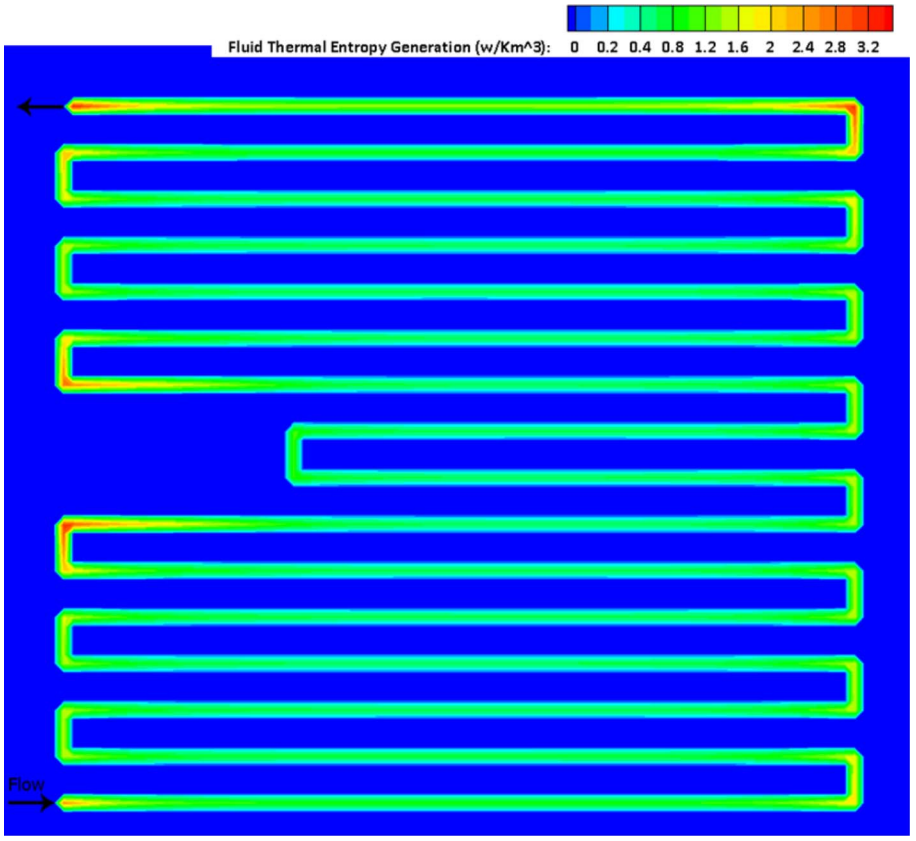

Fig. 17. The thermal entropy generation distribution in the collector for Al_2O_3/water 0.2 wt%.

5. Conclusion

This study numerically investigates the effect of mass fraction of various nanofluids on the entropy generation of a PVT system. The effects of nanofluids on thermo-physical properties, energy and exergy efficiencies were also examined. For the numerical part, Al_2O_3, TiO_2, ZnO and SiO_2 /water nanofluids with various mass fractions up to 10 wt % in a constant mass flow rate were studied. Important findings of this study are summarized as follows:

- By increasing the mass fraction of metallic nanofluids considered in this study, frictional entropy generation was decreased. ZnO /water had the lowest frictional entropy generation among considered nanofluids. This nanofluid with a mass fraction of 10 wt% reduced the frictional entropy generation by 10.87% compared to that of pure water.
- For the metalloid nanofluid, however, a reverse effect was obtained. SiO_2 /water showed the highest frictional entropy generation among considered nanofluids. This nanofluid with a mass fraction of 10 wt % increased the frictional entropy generation by 0.94% compared to that of pure water.
- The effects of adding nanoparticles on the reduction of thermal entropy generation were more pronounced compared to that of the frictional entropy generation.

- Al_2O_3 /water had the lowest thermal entropy generation. This nanofluid with a mass fraction of 10 wt% reduced the thermal entropy generation by 6.24% compared to that of pure water.
- Compared to other nanofluids, Al2O3/water generated the least total entropy generation. The frictional entropy generation for this nanofluid, however, was not desirable compared to other metallic nanofluids studied in this paper.
- Adding metallic nanofluids can decrease the pressure drop that has an effect on pumping power which is favorable. Also, it is found that the metalloid nanofluid (SiO_2/water) can increase the pressure drop which is undesirable.
- For a constant mass flow rate, adding nanoparticle increased density (the lowest for SiO_2/water, highest for ZnO/water), viscosity (the highest for SiO_2/water, lowest for ZnO/water) and thermal conductivity (the highest for Al_2O_3/water, lowest for SiO_2/water). The specific heat capacity, however, was almost the same for all studied nanofluids.
- In constant mass flow rate, adding nanoparticle decreased the Reynolds number (the highest for ZnO/water, lowest for SiO_2 /water) While adding metallic nanoparticles decreased the Prandtl number, the metalloid nanofluid had negligible variation in the Prandtl number.
- For a laminar flow with constant mass flow rate, by increasing the mass fraction the Nusselt was decreased. The heat transfer coefficient of fluid, however, was increased (Al_2O_3/water is highest and SiO_2 /water is lowest). Therefore, for prediction of the heat transfer in nanofluids, the heat transfer coefficient should be used not the Nusselt number.
- Adding nanoparticle improved the thermal exergy efficiency of the system. ZnO/water had the highest and SiO_2/water had the lowest thermal exergy efficiency. These two nanofluids improved the thermal exergy by 10.39% and 9.94% compared to that of pure water, respectively.
- Increasing mass fraction had little improvements in electrical exergy efficiency compared to that of the pure water (the enhancement of electrical exergy efficiency is 1.18%, 1.16%, 1.23% and 1.11% for Al_2O_3, TiO_2, ZnO and SiO_2 /water nanofluids by 10 wt% compared to those of pure water, respectively).ZnO/water has the highest total exergy compared to other nanofluids.

In general, regardless of the economic aspect of nanofluid preparation, using nanofluids can enhance the performance of a PVT based nanofluid collector based on 1st and 2nd laws of thermodynamic. From entropy generation view point, metallic nanofluids due to their thermophysical properties show a better performance compared to metalloid nanofluid.

References

[1] Tian Y, Zhao C-Y. A review of solar collectors and thermal energy storage in solar thermal applications. Appl Energy 2013;104:538–53.
[2] Sardarabadi M, Passandideh-Fard M, Zeinali Heris S. Experimental investigation of the effects of silica/water nanofluid on PV/T (photovoltaic thermal units). Energy 2014;66:264–72.
[3] Luque A, Hegedus S. Handbook of photovoltaic science and engineering. John Wiley & Sons; 2011.
[4] Skoplaki E, Palyvos J. On the temperature dependence of photovoltaic module electrical performance: a review of efficiency/power correlations. Sol Energy 2009;83(5):614–24.
[5] Kalogirou SA, Tripanagnostopoulos Y. Hybrid PV/T solar systems for domestic hot water and electricity production. Energy Convers Manage 2006;47(18):3368–82.
[6] Chow TT. A review on photovoltaic/thermal hybrid solar technology. Appl Energy 2010;87(2):365–79.
[7] Zhang X, Zhao X, Smith S, Xu J, Yu X. Review of R & D progress and practical application of the solar photovoltaic/thermal (PV/T) technologies. Renew Sustain Energy Rev 2012;16(1):599–617.
[8] Bhattarai S, Oh J-H, Euh S-H, Krishna Kafle G, Hyun Kim D. Simulation and model validation of sheet and tube type photovoltaic thermal solar system and conventional solar collecting system in transient states. Solar Energy Materials and Solar Cells 2012; 8(103): p. 184–93.
[9] Rejeb O, Dhaou H, Jemni A. A numerical investigation of a photovoltaic thermal (PV/T) collector. Renew Energy 2015.
[10] Yazdanpanahi J, Sarhaddi F, Adeli MM. Experimental investigation of exergy efficiency of a solar photovoltaic thermal (PVT) water collector based on exergy losses. Solar Energy 2015.
[11] Singh S, Agrawal S. Parameter identification of the glazed photovoltaic thermal system using Genetic Algorithm-Fuzzy System (GA–FS) approach and its comparative study," Energy Conversion and Management 2015; 2015/11/15(105): p. 763–71.
[12] Singh S, Agrawal S. Efficiency maximization and performance evaluation of hybrid dual channel semitransparent photovoltaic thermal module using fuzzyfied genetic algorithm. Energy Conv Manage 2016; 2016/08/15(122): p. 449–61.
[13] Yazdanifard F, Ebrahimnia-Bajestan E, Ameri M. Investigating the performance of a water-based photovoltaic/thermal (PV/T) collector in laminar and turbulent flow regime. Renew Energy 2016.
[14] Rejeb O, Sardarabadi M, Ménézo C, Passandideh-Fard M, Dhaou MH, Jemni A. Numerical and model validation of uncovered nanofluid sheet and tube type photovoltaic thermal solar system. Energy Conv Manage, Article 2016;110:367–77.
[15] Sardarabadi M, Passandideh-Fard M. Experimental and numerical study of metal-oxides/water nanofluids as coolant in photovoltaic thermal systems (PVT). Solar Energy Mater Solar Cells 2016.
[16] Khanjari Y, Pourfayaz F, Kasaeian AB. Numerical investigation on using of nanofluid in a water-cooled photovoltaic thermal system. Energy Conv Manage 2016.
[17] Tagliafico LA, Scarpa F, De Rosa M. Dynamic thermal models and CFD analysis for flat-plate thermal solar collectors – a review. Renew Sustain Energy Rev 2014; Feb 2(30): p. 526–37.
[18] Oztop HF, Al-Salem K. A review on entropy generation in natural and mixed convection heat transfer for energy systems, Renew Sustain Energy Rev 2012;Jan 1(16): p. 911–20.
[19] Moghaddami M, Shahidi S, Siavashi M. Entropy generation analysis of nanofluid flow in turbulent and laminar regimes. J Comput Theor Nanosci 2012;9(10):1586–95.
[20] Alim, et al. Analyses of entropy generation and pressure drop for a conventional flat plate solar collector using different types of metal oxide nanofluids. Energy and Buildings 2013.
[21] Mahian O, et al. A review of entropy generation in nanofluid flow. Int J Heat Mass Transf 2013;65:514–32.
[22] Drew DA, Passman SL. Theory of multicomponent fluids. Springer Science & Business Media, 2006.
[23] Brinkman H. The viscosity of concentrated suspensions and solutions. J Chem Phys 1952;20(4). 571-571.
[24] Maxwell JC. A treatise on electricity and magnetism. Clarendon press, 1881.
[25] Swinbank WC. Long-wave radiation from clear skies. Quarterly J Royal Meteorol Soc 1963;89(381):339–48.
[26] McAdams WH. Heat transmission. 3rd ed., New York: McGraw-Hill; 1954.
[27] Qiu Z, Zhao X, Li P, Zhang X,Ali S, Tan J. Theoretical investigation of the energy performance of a novel MPCM (Microencapsulated Phase Change Material) slurry based PV/T module. Energy, 2015.
[28] Daungthongsuk W, Wongwises S. A critical review of convective heat transfer of nanofluids. Renew Sustain Energy Rev 2007;11(5):797–817.
[29] Bejan A. Entropy Generation Through Heat and Fluid Flow, Wiley, New York. 1982.
[30] White FM. Fluid Mechanics. In: White Frank M, editor, McGraw-hill, 2003.
[31] Mahian O, Kianifar A, Sahin AZ, Wongwises S. Entropy generation during Al_2O_3/water nanofluid flow in a solar collector: effects of tube roughness, nanoparticle size, and different thermophysical models. Int J Heat Mass Transf 2014;78:64–75.
[32] Said Z, Saidur R, Rahim NA, Alim MA, Analyses of exergy efficiency and pumping power for a conventional flat plate solar collector using SWCNTs based nanofluid. Energy and Buildings, 2014;8(vol. 78):p. 1–9.
[33] Wen D, Lin G, Vafaei S, Zhang K. Review of nanofluids for heat transfer applications. Particuology 2009;7(2):141–50.
[34] Faramarz S, Said F, Hossein A, Amin B. Exergetic optimization of a solar photovoltaic array, J Thermody, vol. 2009, 2010.
[35] Yazdanpanahi J, Sarhaddi F, Mahdavi Adeli M. Experimental investigation of exergy efficiency of a solar photovoltaic thermal (PVT) water collector based on exergy losses. Sol Energy 2015;118:197–208.
[36] Sobhnamayan F, Sarhaddi F, Alavi MA, Farahat S, Yazdanpanahi J. Optimization of a solar photovoltaic thermal (PV/T) water collector based on exergy concept. Renew Energy 2014;68:356–65.
[37] Bhattarai S, Kafle GK, Euh S-H, Oh J-H, Kim DH. Comparative study of photovoltaic and thermal solar systems with different storage capacities: performance evaluation and economic analysis. Energy 2013;61:272–82.
[38] Faizal M, Saidur R, Mekhilef S, Alim MA. Energy, economic and environmental analysis of metal oxides nanofluid for flat-plate solar collector. Energy Convers Manage 2013;76:162–8. 2013/12/01/ 2013.
[39] The Last Version of Iranian National Energy Sheet -2016, http://pep.moe.gov.ir/.
[40] Bernal-Agustín JL, Dufo-López R. Economical and environmental analysis of grid connected photovoltaic systems in Spain. Renew Energy 2006;31(8):1107–28.